Thank you for your recent order purchased through FIZ AutoDoc and delivered by Infotrieve.

If you have any questions or problems, contact FIZ AutoDoc Service at:

Tel: +49 7247 808333
Fax: +49 7247 808135
Email: autodoc@fiz-karlsruhe.de
Web site: http://autodoc.fiz-karlsruhe.de/

ORDER INFORMATION SUMMARY:

STN-K-2623158-4525406

Infotrieve Order ID: 859033 / Cart ID: 480818
Copies: 1
Ordered By: FIZ Karlsruhe
Ordered By Email: autodoc@fiz-karlsruhe.de
Order Time: 11/19/2010 1:45 PM
Originally Promised By: 11/22/2010 1:45 PM
Urgency: Normal
Genre: Article
Type: Doc Del (Journal Article)
Usage: 1 copy will be made in your location for the following use: "Internal General Business Use"

ARTICLE INFORMATION:
00042056
Chemica scripta
9/, 1976
Rolf Sjoeblom
Hydrogen bond studies 114

Chemica Scripta. 1976, 9, 127–132

Hydrogen Bond Studies

114. ***A wide-line and pulse proton magnetic resonance study of molecular motion in solid dimethylammonium chloride***[1]

Rolf Sjöblom

Institute of Chemistry, University of Uppsala, Uppsala, Sweden

Received November 5, 1975

Abstract

Hydrogen bond studies. 114. A wide-line and pulse proton magnetic resonance study of molecular motion in solid dimethylammonium chloride. Sjöblom, R. (Institute of Chemistry, University of Uppsala, P.O. Box 531, S-751 21 Uppsala, Sweden).
Chemica Scripta (*Sweden*) 1976, 9 (3), 127–132..

Wide-line PMR data are reported for monocrystalline dimethylammonium chloride near and above room temperature. It is concluded from comparisons between experimental and theoretical second moments that the methyl groups reorient comparatively rapidly, and that the cation as a whole reorients around two different axes. One axis is close to the symmetry axis of the free cation, and the other is parallel to the carbon–carbon direction. Further support for these conclusions are obtained from PMR relaxation times recorded over the temperature range 130–440 K. Some of the relaxation constants, time factors and activation barriers of the different motions in the three phases exhibited by this compound are also reported.

Introduction

Differential thermal analysis indicate two phase transitions in dimethylammonium chloride (DMAC): one at 313 K and another at 260 K [1]. The phases are denoted α, β and γ on going from high to low temperature, in accordance with Ref. [2].

The crystal structures of β-DMAC [3] (cf. Fig. 1) and α-DMAC [2] have been determined by X-ray diffraction, but the crystal structure of the γ-phase is not known. The cations in α-DMAC are disordered around axes parallel to the carbon–carbon directions and close to the centres of mass. These axes are parallel to the c axis in Fig. 1. The short range structure is almost the same in β-DMAC as in α-DMAC [2], and the cells and symmetries of the two phases are accordingly closely related [2, 3]: β-DMAC is orthorhombic and α-DMAC is tetragonal, with space groups *Ibam* and *I4/mmm*, respectively.

The molecular motions in DMAC have been investigated by wide-line NMR by two groups of workers independently: Andrew and Canepa [4], and Sjöblom and Tegenfeldt [5]. Two narrowings were observed [5] in the second moment vs. temperature curve, indicating the onset of methyl group reorientations at low temperatures and reorientations of the cations as a whole around room temperature. The high temperature value of the second moment is too small to be accounted for by reorientations of the cations around their pseudo-symmetry axes alone [4]. Accordingly, and in view of the similarities between β-DMAC [3] and α-DMAC [2], a model was proposed [5] where the cations reorient about axes parallel to the crystallographic c axes of the two phases (i.e., axes parallel to the carbon–carbon directions of the cations; cf. Fig. 1). This model implies that the motions are highly correlated in the β-phase, where a rigid structure has been observed by X-ray diffraction [3, 5].

The purpose of this study is to provide further information about the reorientational motions in DMAC and their associated activation barriers.

Experimental

Commercially obtained DMAC was recrystallized three times from ethanol. The first "single crystal" was grown from the melt as described in Ref. [3]. This procedure gives single crystals in the α-phase which develop random microtwinning when they transform into their β-phase [3] which is stable at room temperature. The twinning is such that the a and b axes (cf. Fig. 1) of one crystallite are closely parallel to the b and a axes, respectively, of another crystallite in the twinned orientation. Large and well shaped single crystals were therefore grown from a saturated solution of DMAC in ethanol over a period of several months.

The registration of wide-line spectra and the evaluation of experimental second moments have been described previously [5, 6]. These measurements were made on a Varian Asc. wide-line NMR spectrometer. The relaxation times were evaluated, as described earlier [7], from the free induction decay following 180°–90° pulses on a Bruker B-KR 322 s variable frequency NMR

[1] Part 113: Acta Crystallogr. *1976*, **B** 32, 232.

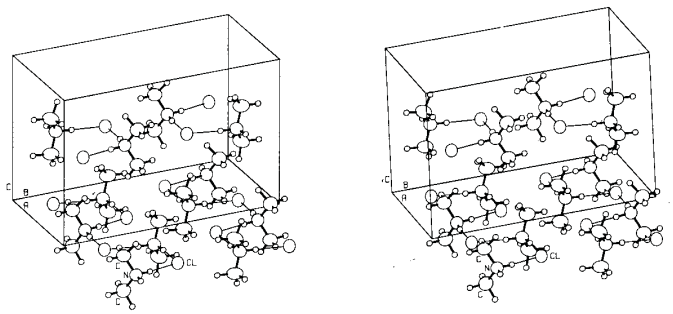

Fig. 1. The crystal structure of β-DMAC. The hydrogen bond chains are parallel to the crystallographic a-axis.

Table I. *The functions q_i used to extract the orientational dependence of the second moment from the second moment tensor*

The vector $\mathbf{h}=(x, y, z)$ is a unit vector parallel to the external magnetic field and given in an orthonormal basis system **i**, **j** and **k**. These are in the present case parallel to the crystallographic basis vectors **a**, **b** and **c**, respectively

$q_1=(5/4)^{\frac{1}{2}}(1-3z^2)$	$q_4=15^{\frac{1}{2}}xz$
$q_2=(15/4)^{\frac{1}{2}}(x^2-y^2)$	$q_5=15^{\frac{1}{2}}yz$
$q_3=15^{\frac{1}{2}}xy$	

spectrometer at the University of Nottingham. The calculations were carried out on ICL 1906A and IBM 1800 computers.

The phase changes could readily be studied during the experimental work on the pulse spectrometer, and the observation could be made that the phase transition between the α- and the β-phase is reversible and is always found to take place within minutes. On the other hand, it was found that under certain circumstances, the β- to γ-phase transition could be readily prevented.

Thus, a sample which had been dried under vacuum by continuous pumping for several days did not transform to the γ-phase even if it was cooled to temperatures far below the transition temperature. If a dry sample was exposed to the air for a few seconds (the compound is hygroscopic) and then dried under vacuum for only a few hours, then the β to γ transformations took place within minutes. The transformation from the γ- to the β-phase was always found to take place relatively quickly.

Theoretical second moments

The general procedure used for the calculation of second moments is described in Ref. [8] (see also Refs. [9, 10 and 11]) and will therefore only be briefly reviewed. The second moment of a solid, M_2, can be written as a quadratic form $M_2=\tilde{\mathbf{q}}\mathbf{S}\mathbf{q}$, where **S** is the second moment tensor which depends only on the crystal structure and the assumed motion. Furthermore, $q_i=2\sqrt{\pi}\phi_i(\mathbf{h})$ where ϕ_i are the real second-order spherical harmonics listed in Table I, and **h** is a unit vector parallel to the external magnetic field. The powder average is simply the trace of the second moment tensor.

The atomic coordinates used were obtained in the following way. The cation in dimethylammonium hydrogen oxalate (as determined from X-ray diffractometer data [12]) was transformed isometrically into the structure of β-DMAC (which was determined from visually estimated X-ray data [3]) in such a way that the three non-hydrogen atoms coincided as closely as possible. The hydrogen positions obtained in this way were then further modified by elongations of the C–H and the N–H bonds by 0.13 and 0.06 Å, respectively. This takes account of the well-known systematic displacement of hydrogen atom positions as determined by X-ray diffraction [13]. The distance between the hydrogen atoms in a methyl group and in an NH_2 group were furthermore given the values 1.79 and 1.68 Å in all calculations of the intra-group contributions to the second moment [5]. The calculations included the twelve nearest neighbouring cations, and contributions from atoms further out were estimated as described earlier [5].

The following models were used for the reorientational motions in DMAC:

(*a*) Reorientations of the methyl groups around their three-fold pseudo-symmetry axes.

(*b*) Reorientations of the cations as a whole around their two-fold pseudo-symmetry axes.

(*c*) Reorientations of the cations as a whole around their carbon–carbon directions. The motions are strongly correlated so that the structure of β-DMAC is preserved at any instant (except for the short time during which the reorientations take place). Thus, a part of the crystal changes between the configurations illustrated in Figs. 2*a*, 2*b*, 2*c* and 2*d*.

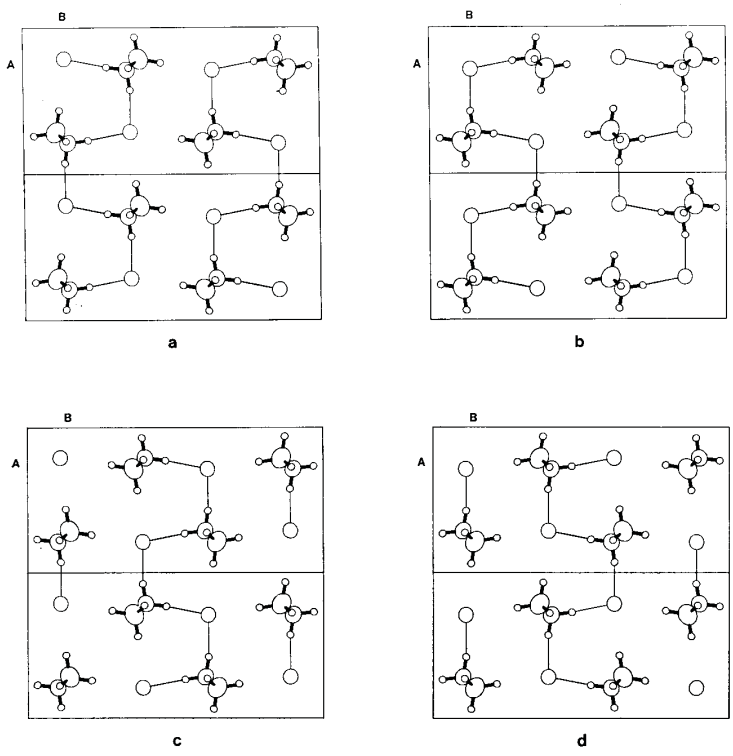

Fig. 2. According to model *c*, the structure will change between the configurations *a*, *b*, *c* and *d*. Model *d* implies changes between the configurations *a* and *b* only. The layers above and below (cf. Fig. 1) are assumed to change correspondingly.

Table II. *Theoretical second moment tensors (for β-DMAC) in G² for various possible combinations of motions (cf. text)*

$S_{12}=S_{21}$; other elements not listed are zero. The results for models $a+c$ and $a+b+c$ are the same as those for $a+c+d$ and $a+b+c+d$, respectively

Model	Contributing part	S_{11}	$2S_{12}$	S_{22}	S_{33}	S_{44}	S_{55}
Rigid	Intra cation	4.755	−0.081	4.794	8.827	4.251	4.313
	Total	5.414	−0.064	5.451	9.479	4.944	5.083
a	Intra cation	3.035	−0.095	0.538	3.848	2.255	2.288
	Total	3.359	−0.117	0.947	4.312	2.771	2.799
a+b	Intra cation	3.009	−0.079	0.004	3.843	0.184	0.167
	Total	3.250	−0.055	0.221	4.234	0.455	0.468
a+c	Intra cation	3.031	−0.103	0.009	0.001	0.000	0.001
	Total	3.260	−0.119	0.344	0.369	0.426	0.444
a+d	Intra cation	3.031	−0.103	0.010	0.001	0.170	2.120
	Total	3.293	−0.114	0.370	0.415	0.616	2.599
a+b+c	Intra cation	3.005	−0.078	0.003	0.001	0.000	0.000
	Total	3.193	−0.075	0.170	0.342	0.249	0.258
a+b+d	Intra cation	3.005	−0.079	0.004	0.001	0.169	0.003
	Total	3.207	−0.074	0.188	0.369	0.421	0.272

(*d*) Reorientations similar to the ones in (*c*) but more restricted, so that a part of the structure only changes between the configurations illustrated in Figs. 2*a* and 2*b*.

This labelling of the models for the motions will be used throughout this paper.

A rigid structure was observed by X-ray diffraction for β-DMAC. Motions according to models *c* and *d* are possible in this phase only if they are strongly correlated so that, at a certain instant, the translational symmetry is perfect within most of the mosaic blocks. This point is discussed in further detail in Ref. [5], where a model for the changes is proposed which includes boundaries containing disordered structure (perhaps α-phase) which move about in the crystal and cause the observed configurational changes.

Second moment tensors were calculated for β-DMAC using the program PSM [10, 11] for various plausible combinations of the different reorientational motions, and the results are listed in Table II. Estimates of the corresponding second moment tensors in the α-phase may readily be obtained by putting $S_{12}=0$ and $S_{44}=S_{55}$ (= the average of S_{44} and S_{55} for the β-phase) since the structures of α- and β-DMAC are very similar [2]. It may be interesting to note that the intramolecular second moment tensor for model $a+b+c$ is about the same as that obtained on the assumption that a cation reorients freely around an axis parallel to the *c* axis together with reorientations about all two-fold axes in the mirror plane of the molecule perpendicular to this axis.

The calculations have only concerned the simple cases where the rate of a particular motion is either slow or fast compared to the linewidth. Intermediate cases are discussed later in this paper.

Experimental second moments

Experimental second moments were measured for various directions of the magnetic field in a plane of the microtwinned crystal at 298, 343 and 368 K. Similar measurements were also made at 298 and 343 K for a different orientation axis of the single crystal. Only a limited range of second moments were determined at the latter temperature since the crystal was accidentally damaged. The experimental second moment vs. orientation angle are shown in Figs. 3*a* and 3*b* for the microtwinned and single crystals, respectively.

The orientation axes for the two mountings used were determined by least-squares, using in each case the observed setting angles for about ten reflexions on a four-circle X-ray diffractometer. The reference directions together with the experimental second moment tensor for the α-phase were determined in a least-squares procedure using the program ESM [11]. Forty-seven second moments recorded at 343 and 368 K could be included in the refinement since the second moment varies only slightly with temperature in this region. The quantity minimized, *R*, was the r.m.s. value of $(M_2(\text{obs.})-M_2(\text{calc.}))/M_2(\text{calc.})$, and its final value became 0.042. The constraints on the second moment tensor for *4/mmm* symmetry given in Refs. [8] and [9] were used. The result of the refinement is given in Table III and in Fig. 3, where the lower solid lines are calculated from the experimental second moment tensor.

Second moments for various models based on the theoretical second moment tensors in Table II vs. the orientation angles are illustrated in Figs. 4*a* and 4*b* for the orientations of the microtwinned and single crystals, respectively. These curves may be compared with the experimental ones in Fig. 3*a* and 3*b*. (It should be observed, that tetragonal symmetry is assumed in Fig. 4*a*.)

The experimental second moments for the α-phase agree

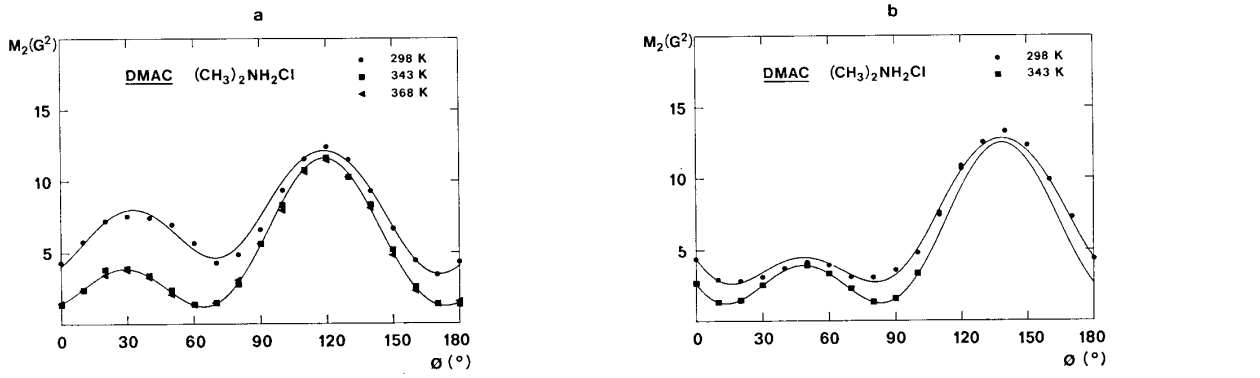

Fig. 3. The experimental second moments vs. orientation angle for the microtwinned (3a) and the single crystal (3b) at different temperatures. The microtwinned crystal (3a) was mounted around an axis (0.12283, −0.02831, 0.01651); the angle $\phi=0°$ corresponds to $\mathbf{h}=(-0.03996, -0.05702, -0.04830)$ and $\phi=90°$ to $\mathbf{h}=(-0.04556, -0.02633, 0.08686)$. The vectors are expressed in fractional coordinates. The single crystal (3b) was mounted about an axis (−0.13676, −0.00359, −0.00162); the angle $\phi=0°$ corresponds to $\mathbf{h}=(-0.00307, 0.04553, -0.07558)$ and $\phi=90°$ to $\mathbf{h}=(-0.00681, 0.05158, 0.06660)$. The lower solid curve is calculated from the experimental second moment tensor for the α-phase, and the upper solid curve corresponds to the M_2(calc.) from the best fit in the line narrowing analysis (cf. text).

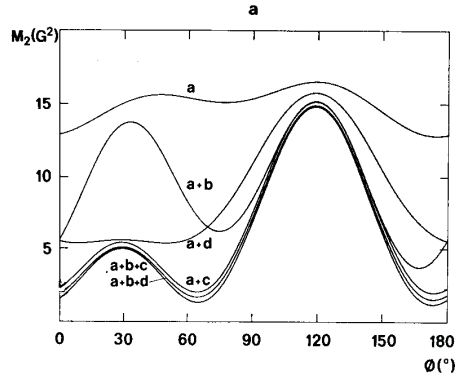

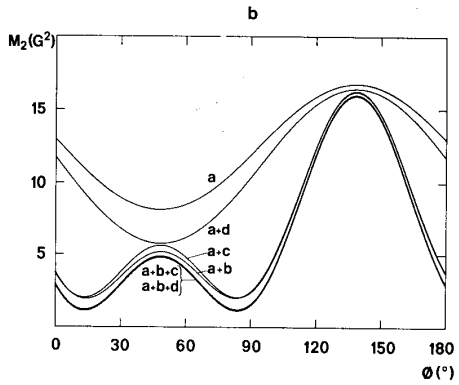

Fig. 4. The theoretical second moment for various models for the motions vs. the experimentally used orientation angles. The second moments are calculated from the second moment tensors in Table II. The angles in Figs. 4*a* and 4*b* have the same meaning as those in Figs. 3*a* and 3*b*, respectively.

reasonably well with the theoretical ones for models $a+c$, $a+b+c$ and $a+b+d$. The largest disagreement appears for the component S_{11} of the second moment tensor which is much larger than the others and which depends mainly on the intramolecular contributions. This difference may well be explained by vibrational motions which cause a non-negligible decrease of the second moment, as discussed in Ref. [8].

The contributions to the second moments from S_{11} are smallest for the orientations corresponding to the minima of the second moment for the α-phase vs. orientation angle curves in Fig. 3. The theoretical second moments for the single crystal at $\phi = 83°$ (based on the tensors given in Table II together with the symmetry constraints $S_{12}=0$ and $S_{44}=S_{55}$) are 2.02, 1.13 and 1.47 G^2 for the models $a+c$, $a+b+c$ and $a+b+d$, respectively. The value obtained from the experimental second moment tensor is 1.22 G^2, and the model $a+b+c$ thus gives the closest agreement between theory and experiment. This model is also preferable to the model $a+b+d$ in view of the dynamical disorder in the α-phase which makes the directions *a* and *b* equivalent. Further support for this assignment is obtained later in this paper from analyses of the line-narrowing process and the relaxation data.

The line-narrowing process

The second moment decreases with increasing temperature in the entire stability range of the β-phase [4, 5] and we are thus concerned with only partially narrowed NMR spectra in this phase.

It has been shown [14–17] that the narrowing of the NMR line due to one reorientational process follows the relation

$$M_2 = M_2(\text{motion}) + (M_2(\text{rigid}) - M_2(\text{motion})) \cdot \frac{2}{\pi} \tan^{-1}(\alpha\tau M_2^{1/2}) \quad (1)$$

where M_2 is the second moment, α is a constant which for convenience is taken as unity, and τ is the correlation time at the temperature in question. M_2(rigid) is the second moment of the rigid structure, and M_2(motion) is the second moment averaged over the motion.

The situation in the present case is a bit more complex, however. There are four kinds of motions *a*, *b*, *c* and *d* which may be responsible for the narrowing observed in the β-phase. Of these, motion *a* can be excluded since it has been shown [5] that it causes a narrowing only at low temperatures (in the region 110–170 K).

It is shown in Ref. [8] that the dipolar coupling can be divided into different parts, $K_i^{(0)}$ (the superscript will be dropped in the following), where each part has its specific correlation time. The result of such an analysis for the present case is given in Table IV, where the K_i for various motions *b*, *c* and *d* and combinations of these motions are given together with their respective correlation times (the numerical values of the powder averages over K_i, $\bar{K}_i$, are also given). Each of these parts may be assumed to affect the observed second moment according to formula (1) and the result is:

Table III. *The experimental second moment tensor in G^2 for the α-phase*

The symmetry implies that $S_{44}=S_{55}$; other elements not listed are zero. The standard deviations are based on the least-squares refinement only

R	S_{11}	S_{22}	S_{33}	S_{44}
0.042	2.50 ±0.03	0.204 ±0.014	0.184 ±0.017	0.265 ±0.007

Table IV. *Expressions for the correlation times of the various processes or combinations of processes together with the dependencies of the corresponding constants K on the second moments*

It has been assumed that τ_a is much smaller than the other correlation times. Numerical values for the powder averages over (2/3)*K* based on the theoretical second moment tensors in Table II are also given

Correlation time	The relations between *K* and M_2		$(2/3)\bar{K}$ 10^8 s^{-2}
τ_a	$K(a)$	$= M_2$ (rigid) $- M_2(a)$	77.21
τ_b	$K(b)$	$= M_2(a+c+d) - M_2(a+b+c+d)$	3.011
τ_c	$K(c)$	$= M_2(a+b+d) - M_2(a+b+c+d)$	1.169
τ_d	$K(d)$	$= M_2(a+b+c) - M_2(a+b+c+d)$	0
$(\tau_b^{-1}+\tau_c^{-1})^{-1}$	$K(b+c)$	$= M_2(a+d) - M_2(a+b+d) - M_2(a+c+d) + M_2(b+c+d)$	10.52
$(\tau_b^{-1}+\tau_d^{-1})^{-1}$	$K(b+d)$	$= M_2(a+c) - M_2(a+b+c) - M_2(a+c+d) + M_2(a+b+c+d)$	0
$(\tau_c^{-1}+\tau_d^{-1})^{-1}$	$K(c+d)$	$= M_2(a+b) - M_2(a+b+c) - M_2(a+b+d) + M_2(b+c+d)$	19.90
$(\tau_b^{-1}+\tau_c^{-1}+\tau_d^{-1})^{-1}$	$K(b+c+d)$	$= M_2(a) - M_2(a+b) - M_2(a+c) - M_2(a+d) + M_2(a+b+c) + M_2(a+b+d) + M_2(a+c+d) - M_2(a+b+c+d)$	13.00

Table V. *The results of the least-squares refinements of the correlation times τ_b, τ_c and τ_d at 298 K in the β-phase for various assumptions and constraints for the line-narrowing processes*

The standard deviations are based on the refinements only

Assumed motion in α-phase	R=RMS (obs.-calc.)/ calc.)	τ_b $\cdot 10^{-6}$ s	τ_c $\cdot 10^{-6}$ s	τ_d $\cdot 10^{-6}$ s
$a+c+d$	0.094	∞^a	7.03±0.03	∞
$a+b+c+d$	0.059	4.9±2.2	56±232	15±15
	0.059	4.6±0.3	∞^a	11.2±0.7
	0.061	7.0±0.7	11.5±0.9	∞^a
	0.190	1.4±0.6	∞^a	∞^a
	0.149	∞^a	4.8±0.4	∞

[a] Constrained variable.

$$0.5\pi\, M_2 = 0.5\pi\, K(0) + K(b)\tan^{-1}(\delta\tau_b) + K(c)$$

$$\tan^{-1}(\delta\tau_c) + K(d)\tan^{-1}(\delta\tau_d) + K(b+c)\tan^{-1}(\delta\tau_{bc})$$

$$+ K(b+d)\tan^{-1}(\delta\tau_{bd}) + K(c+d)\tan^{-1}(\delta\tau_{cd})$$

$$+ K(b+c+d)\tan^{-1}(\delta\tau_{bcd})$$

$$\text{where}\quad \delta = M_2^{1/2} \tag{2}$$

It turns out that $K(d) = K(b+d) = 0$ for any direction of the magnetic field.

This formula was used in a least-squares refinements of τ_b, τ_c and τ_d in which the quantity minimized, R, was the r.m.s. value of $(M_2(\text{obs.}) - M_2(\text{calc.})/M_2(\text{calc.})$ for the 36 experimentally used orientations (cf. Fig. 3). The M_2(obs.) used (M_2 in formula (2)), were the experimentally obtained second moments at 298 K. The M_2(calc.) were evaluated according to the right hand side of formula (2) using the theoretical second moment tensors (cf. Table II). The totally reduced second moments in the β-phase are approximately the same as those of the α-phase (cf. theoretical second moments), and could thus be calculated from the experimental second moment tensor for the α-phase. Various constraints on the parameters τ_b, τ_c and τ_d were used in the refinements where two models were also used for the narrowed second moment tensor in the α-phase: $a+b+c$ and $a+c$ (which give the same second moments as $a+b+c+d$ and $a+c+d$, respectively). The results of these refinements are shown in Table V. It was found as expected, that the parameters τ_c and τ_d were very highly correlated, and that one of them could often be constrained to any value within a large interval without appreciable shifts in the R-value.

A fairly good fit (R = 0.094) was obtained using the assumption that the second moments in the α-phase are narrowed only by motions a and c and that the broadening of the lines is caused by an increase in τ_c alone. The fits became substantially better, however (R = 0.059–0.061) on making the assumption that the second moments in the α-phase are narrowed by motions a, b and c (or a, b, c and d) and that the broadening is caused by increase in τ_b, τ_c and τ_d. The relative importance of τ_c and τ_d could not be determined, however, since these parameters are very highly correlated. The upper solid lines in Figs. 3*a* and 3*b* show M_2(calc.) for the latter model as a function of the experimentally used orientation angles of the microtwinned and single crystal, respectively.

In conclusion, the motions a, b and c occur in the α-phase and have correlation times smaller than those corresponding to the linewidths. In addition to motion a, the motions b and c, b and d, or b, c and d are present in the β-phase and contribute to the observed line-narrowing.

The relaxation times

Expressions for the relaxation time in the laboratory frame, T_1, in the presence of several reorientational processes are given in Ref. [8], and the result for a polycrystalline sample is in the present case:

$$T_1^{-1} = \sum_{i=1}^{n} \frac{2}{3}\bar{K}_i\left[\frac{\tau_i}{1+\omega_0^2\tau_i^2} + \frac{4\tau_i}{1+4\omega_0^2\tau_i^2}\right] \tag{3}$$

where $\frac{2}{3}\bar{K}_i$ is the relaxation constant and τ_i the correlation time for a single or combined process. Formulae for τ_i and theoretical expressions and values of the corresponding $\bar{K}_i$ are given in Table IV. It has been assumed that the correlation time for the reorientations of the methyl groups is much smaller than for the others.

It appeared during the analysis of the experimental data that an expression involving only single processes and thus simpler than that presented in eq. (3) was sufficient, namely

$$T_1^{-1} = \sum_{i=1}^{n} C_i\left[\frac{\tau_i}{1+\omega_0^2\tau_i^2} + \frac{4\tau_i}{1+4\omega_0^2\tau_i^2}\right] \tag{4}$$

together with the usually assumed expression for the correlation time $\tau_i = \tau_{0i}\exp(E_i/kT)$, where C_i is the experimental relaxation constant for process i, τ_{0i} is the time factor, and E_i the activation barrier. The underlying theory for formula (4) (n = 1) can be found in Refs. [14] and [16].

Formula (4) was used in a least-squares analysis of C_i, τ_{0i} and E_i from the experimental relaxation times obtained for the α-phase, the β-phase below 240 K, and the γ-phase. The quantity minimized in each of the three refinements, R, was the r.m.s. value of $(T_1(\text{obs.}) - T_1(\text{calc.}))/T_1(\text{calc.})$ and the results are shown in Table VI and Fig. 5.

The relaxation time decreases with temperature in the high temperature region in the β-phase. According to formula (3) one would therefore expect the relaxation time to be strongly frequency dependent. There is, however, only a minor difference between the relaxation times obtained at 60.16 MHz and those at 20.00 MHz which implies that the theory presented in Ref. [8] cannot be applied successfully in the present case. There are several possible explanations for this behaviour: the presence of α-phase, unusual frequency dependence of the spectral density functions, cross-relaxation between hydrogen and the quadrupole coupled chlorine nuclei, or paramagnetic impurities. The present data are insufficient for a prolonged discussion of these possibilities, however.

The experimental relaxation constants obtained for the β-phase below 240 K and for the γ-phase are 49.0 and 49.2 × 10^8 s^{-2}, respectively (cf. Table VI). These values may be compared with

Table VI. *The results of the least-squares refinements of the BPP-parameters C, τ_0 and E (cf. formula (4)) from the experimental relaxation times*

The standard deviations are based on the refinement only

Phase	Motion	R=RMS (obs.-calc.)/ calc.	C 10^8 s^{-2}	τ_0 10^{-14} s	E kJ/mole
α	b	0.044	2.88±0.04	1.6±0.3	41.5±0.7
	c (cf. text)		45[a]	3.7±0.8	22.9±0.6
β	a	0.047	49.0±0.9	24.8±2.6	11.08±0.15
γ	a	0.053	49.2±0.7	26.7±2.3	14.69±0.14

[a] Constrained variable as estimated from the values in Table IV.

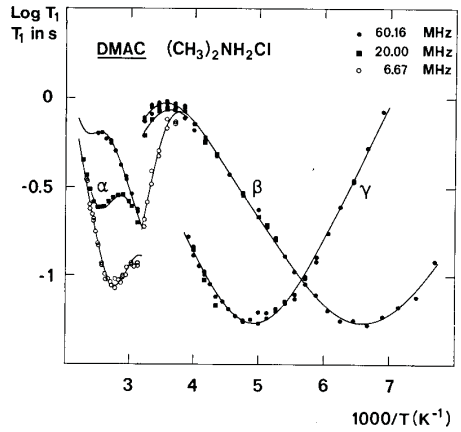

Fig. 5. The 10th logarithm of the experimental relaxation time vs. inverse temperature for the α-, β- and γ-phases. The solid lines were calculated from the parameters given in Table VI. The lines above 240 K in the β-phase are intended only as a visual aid, however.

the theoretical value for motion *a* of 77.2×10^8 s^{-2}. The agreement is reasonable since the high amplitude of torsional vibration of a methyl group reduces the apparent relaxation constant, and since the correlation time for part of the inter-methyl group interactions is actually about one half of the τ_a used [8]. The activation barriers (11.1 and 14.7 kJ/mole for the β- and γ-phases, respectively) are in good agreement with a value obtained from a wide-line study [5] of the γ-phase, 13.8 ± 1.3 kJ/mole, and the barrier for dimethylamine itself, which is 13.5 kJ/mole [18].

At least two processes take place in the α-phase. Only the smallest relaxation constant of 2.88×10^8 s^{-2} was determined experimentally (cf. Table VI). The value is in good agreement with the one for $\frac{3}{8}\bar{K}(b)$ in Table IV. This assignment would imply that $\tau_b > \tau_c$, which is quite reasonable in view of the disorder in the α-phase which should affect τ_c much more strongly than τ_b (it was shown in the preceding section that $\tau_c > \tau_b$ in the β-phase). Such effects have been found earlier for the closely related compounds monomethylammonium chloride [19] and trimethylammonium chloride [7]. The activation barrier for motion *b* in the α-phase is thus 42 kJ/mole. It cannot be concluded from the present data whether the other minimum is caused by motion *c* alone or by both *c* and *d*.

Acknowledgements

The author wishes to thank Dr Jörgen Tegenfeldt, who introduced him to this field, for valuable guidance, suggestions and comments. The author is also grateful for the kind hospitality shown to him by Professor E. R. Andrew and his colleagues at the University of Nottingham, and in particular for the use of his pulse spectrometer. The author finally thanks Professor Ivar Olovsson for generously providing facilities used for this study.

References

1. Stammler, J., Inorg. Nucl. Chem. *1967*, 29, 2203.
2. Lindgren, J. and Arran, N., Acta Chem. Scand. *1972*, 26, 3043.
3. Lindgren, J. and Olovsson, I., Acta Crystallogr. *1968*, B24, 549.
4. Andrew, E. R. and Canepa, P. C., J. Magn. Res. *1972*, 7, 429.
5. Sjöblom, R. and Tegenfeldt, J., Acta Chem. Scand. *1972*, 26, 3068.
6. Tegenfeldt, J. and Olovsson, I., Acta Chem. Scand. *1971*, 25, 101.
7. Sjöblom, R. and Punkkinen, M., J. Magn. Res. *1975*, 20, 491.
8. Sjöblom, R., UUIC-B19-137, J. Magn. Res., in press.
9. Sjöblom, R., 18th Ampere Congress, Nottingham, 1974, p. 485.
10. Sjöblom, R. and Tegenfeldt, J., UUIC-B13-2, Institute of Chemistry, University of Uppsala, Sweden, 1973.
11. Sjöblom, R., UUIC-B13-7, Institute of Chemistry, University of Uppsala, Sweden, 1975.
12. Thomas, J. O. and Pramatus, S., Acta Crystallogr. *1975*, B31, 2159.
13. Almlöf, J., Kvick, Å. and Thomas, J. O., J. Chem. Phys. *1973*, 59, 3901.
14. Bloembergen, N., Purcell, E. M. and Pound, R. V., Phys. Rev. *1948*, 73, 679.
15. Gutowsky, H. S. and Pake, G. E., J. Chem. Phys. *1950*, 18, 162.
16. Kubo, R. and Tomita, K., J. Phys. Soc. Japan, *1954*, 9, 888.
17. Andrew, E. R. and Lipofsky, J., J. Magn. Res. *1972*, 8, 217.
18. Wollrab, J. E. and Laurie, V. W., J. Chem. Phys. *1971*, 54, 532.
19. Tegenfeldt, J. and Ödberg, L., J. Phys. Chem. Solids *1972*, 33, 215.

Institute of Chemistry
University of Uppsala
P.O. Box 531
S-751 21 Uppsala, Sweden